

Memristive Biosensors Under Varying Humidity Conditions

Francesca Puppo*, Akshat Dave, Marie-Agnès Doucey, Davide Sacchetto, Camilla Baj-Rossi, Yusuf Leblebici, *Fellow, IEEE*, Giovanni De Micheli, *Fellow, IEEE*, and Sandro Carrara, *Member, IEEE*

Abstract—We attempt to examine the potential of silicon nanowire memristors in the field of nanobiosensing. The memristive devices are crystalline Silicon (Si) Nanowires (NWs) with Nickel Silicide (NiSi) terminals. The nanowires are fabricated on a Silicon-on-Insulator (SOI) wafer by an Ebeam Lithography Technique (EBL) process that allows high resolution at the nanoscale. A Deep Reactive Ion Etching (DRIE) technique is used to define free-standing nanowires. The close alignment between Silicon (Si) and Nickel-Silicide (NiSi) terminals forms a Schottky-barrier at their junction. The memristive effect of the fabricated devices matches well with the memristor theory. An equivalent circuit reproducing the memristive effect in current-voltage (I-V) characteristics of our silicon nanowires is presented too. The memristive silicon nanowire devices are then functionalized with anti-human VEGF (Vascular Endothelial Growth Factor) antibody and I-V characteristics are examined for the nanowires prior to and after protein functionalization. The uptake of bio-molecules linked to the surface of the memristive NWs is confirmed by the increased voltage gap in the hysteresis curve. The effects of varying humidity conditions on the conductivity of bio-modified memristive silicon nanowires are deeply investigated.

Index Terms—Antibody, biosensor, humidity, memristor, nanofabrication, silicon nanowire.

I. INTRODUCTION

IN RECENT years, electronic detection of biomolecules has become one of the most widely researched topics in nanotechnology. New developments have paved the way to a

Manuscript received January 11, 2013; revised November 18, 2013; accepted December 04, 2013. Date of publication January 14, 2014; date of current version February 27, 2014. The work was in part supported by the multidisciplinary FNS grant (CR3213 135073) and by an ERC grant (ERC-2009-Adg-246810). This work was also partially supported by the Nano-Tera grants no. 20NA21-128841 and no. 20NA21-128840, evaluated by the Swiss NSF foundation. *As-risk indicates corresponding author.*

*F. Puppo is with the Integrated Systems Laboratory, École Polytechnique Fédérale de Lausanne, 1015 Lausanne, Switzerland (e-mail: francesca.puppo@epfl.ch).

A. Dave, D. Sacchetto, C. Baj-Rossi, G. De Micheli, and S. Carrara are with the Integrated Systems Laboratory, École Polytechnique Fédérale de Lausanne, 1015 Lausanne, Switzerland (e-mail: AKSH0006@e.ntu.edu.sg; davide.sacchetto@epfl.ch; camilla.bajrossi@epfl.ch; giovanni.demicheli@epfl.ch; sandro.carrara@epfl.ch).

M.-A. Doucey is with the Division of Experimental Oncology, Université de Lausanne, 1015 Lausanne, Switzerland (e-mail: Marie-Agnes.Doucey@unil.ch).

Y. Leblebici is with the Microelectronic Systems Laboratory, École Polytechnique Fédérale de Lausanne, 1015 Lausanne, Switzerland (e-mail: yusuf.leblebici@epfl.ch).

Color versions of one or more of the figures in this paper are available online at <http://ieeexplore.ieee.org>.

Digital Object Identifier 10.1109/TNB.2013.2295517

large number of novel nano-scale devices of highly promising properties for electrochemical sensor and biosensor applications [1]–[8]. In particular, nanowires have become the focus of intensive research due to their unique properties and their potential for fabrication of nanosensors which can provide fast, low-cost, and high-throughput analysis of biological processes. Nanowires promise to revolutionize many area in medicine and biochemistry, ranging from the detection [9], [10] and diagnosis [11] of diseases to the discovery of new drug delivery systems [12]. Indeed, the electrical properties of nanowires are strongly influenced by minor perturbations [13], [14] because of their high surface-to-volume ratio and because of tunable electron transport properties due to quantum confinement effect, thus offering new capabilities not available in larger scale devices. Unlike 2-D thin films, the charge accumulation or depletion in the 1-D nanostructure takes place in the bulk of the structure thus giving rise to large changes in the electrical properties that potentially enable the detection of a single molecule [15]. Up to now, this property of the 1-D nanostructures has been shown to provide a sensing modality for label-free and direct electrical readout when the nanostructure is used as a semiconducting channel of a chemiresistor or field-effect transistor [16], such as in gas sensors [17] and Ion-Sensitive Field-Effect Transistors (IS-FETs) for cancer markers [9] or DNA [18] detection.

Recently, a completely new insight for biosensing based on the memristive effect of functionalized Schottky-barrier silicon nanowires in dry environment has been reported [19]. Due to the nano-scale of the fabricated geometries [20], silicon nanowire devices have been discovered to show hysteretic properties imputable to memristive devices [21]. In these devices, the memory effect depends on charge carriers re-arrangement at the nanoscale as due to external perturbation. Moreover, nanofabricated memristive silicon nanowires, functionalized with biomolecular films, have been demonstrated to sense varying concentrations of protein solutions thanks to corresponding variations of the hysteresis curve parameters [19]. Nevertheless, only few models has been proposed so far for describing and simulating the memristive effect of silicon nanowires [22]. Moreover, a very significant and uncontrolled dependence of the biosensing mechanism with respect to the environmental conditions has been pointed out [19]. So far, biosensing methods based on silicon nanowires tested in dry experimental conditions have not been reported in literature. The air humidity has revealed one important factor strongly affecting the nanowire biosensor performances in dry environment [19]. Carrara *et al.* have already demonstrated the role of the water shell adsorbed from the surrounding humid

environment to the surface of a layer of rather small organic molecules, supposed not to have internal water [23]. Humidity can introduce noise in experimental measurements with silicon nanowires too, confusing data and thus, leading to unconvincing results of bio-detection. This kind of problem has not been discussed yet. In this study we aimed to face this important issue of nanowire based biosensing in dry environment.

In particular, in this article we show that our memristive silicon nanowires are well fitted by the memristor theory. We also propose an equivalent circuit description emulating the meristive effect of silicon nanowires. Moreover, we investigate the impact of the air relative humidity (rH) on the hysteretic effect of silicon nanowire through an accurate statistical analysis performed on a large number of devices. Each wire was tested before and after their functionalization with anti-human VEGF (Vascular Endothelial Growth Factor) antibody at different humidity values. Thanks to this deep analysis we succeeded in confirming once more the electrical modification of nanofabricated memristors when functionalized with antibodies. Additionally, we identified the role of varying humidity conditions in the modification of the hysteretic voltage gap of bio-modified silicon nanowires.

A. Memristor Nano-Fabrication

Memristive silicon nanowires are obtained through a top-down fabrication process performed on a Silicon-On-Insulator (SOI) wafer with a 350 nm thick device layer. Fig. 1 summarizes some of the critical steps of the process flow. The fabrication starts from the Low Pressure Chemical Vapour Deposition (LPCVD) of low stress $\text{Si}_x\text{N}_y\text{H}_z$ on top of a SOI wafer (Fig. 1(a)). Subsequently, a 50 nm thick Hydrogen Silsesquioxane (HSQ) layer, which is used as negative tone resist for Electron Beam Lithography (EBL), is spin coated onto the substrate. The HSQ is patterned by an EBL process into lines with lengths ranging between 1 μm and 15 μm in steps of 1 μm . The HSQ lines are then transferred into the $\text{Si}_x\text{N}_y\text{H}_z$ layer by a vertical plasma etching (Fig. 1(b)), and used as hard mask for subsequent processing. A standard photo-resist lithography is carried out to define two polymeric areas of 1000 μm^2 partially overlapping the extremities of the $\text{Si}_x\text{N}_y\text{H}_z$ lines (Fig. 1(c)). The sample is loaded into a plasma etching tool and the exposed Si is etched in two steps. First, 50 nm-thick Si is vertically carved from the substrate by an highly directional $\text{SF}_6/\text{C}_4\text{F}_8$ plasma mixture. Then the remaining 250 nm of Si are removed by an alternated Deep Reactive Ion Etching (DRIE) technique which alternates chemical, and thus isotropic, etching of Si with C_4F_8 passivation steps. This leads to the definition of structures consisting of two large Si areas connected by thin Si/ $\text{Si}_x\text{N}_y\text{H}_z$ nanowires laying onto a 500 nm SiO_2 isolation layer (Fig. 1(d)). Although of different lengths, the $\text{Si}_x\text{N}_y\text{H}_z$ hard masks are defined such that the Si nanowires keep an aspect ratio of 1:200. Hence, a 50 nm-thick Ni layer is deposited by e-beam evaporation onto the sample and annealed at 400°C for 20 minutes in N_2 inert atmosphere. The annealing sinters NiSi on those regions where Ni and Si are in contact, leading to the formation of NiSi 1:1 phase junctions. Unreacted Ni is left on top of the SiO_2 bottom layer and on top of the $\text{Si}_x\text{N}_y\text{H}_z$ hard mask. It is worth noticing that Ni cannot deposit

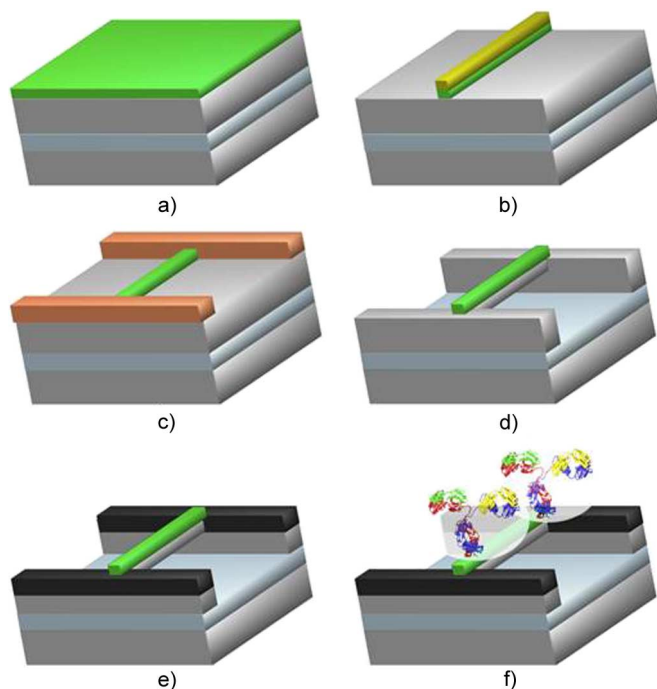


Fig. 1. Process flow related to the fabrication and functionalization of the memristive biosensor.

around the Si nanowires due to the directionality of the e-beam evaporation and the fact that the Si nanowires are less than 50 nm in diameter. The excess Ni is removed with immersion of the samples in a hot Piranha solution for 10 minutes leaving a freestanding Si nanowire anchored between two NiSi pillars (Fig. 1(e)), that are subsequently used as pads for electrical characterization.

We tried also a variant of the fabrication process in which we gave up the use of the $\text{Si}_x\text{N}_y\text{H}_z$ hard mask and proceeded instead with the direct use of the conventional EBL exposure on HSQ pattern lines. After the exposition, the nanowires were obtained as in the process previously explained, by using the alternate DRIE technique. In both processes, by optimizing the timing of the combined etching steps, we obtained either single free-standing silicon nanowires or vertically stacked ones. In Figs. 2 and 3 SEM imaging of the two different configurations is reported. In this case the two images were acquired from wires fabricated through the original process and its variant respectively.

Once fabricated the structures, the nanowires were ready to be functionalized with an anti-human VEGF bio-layer (Fig. 1(f)). More detailed description of the surface modification will be given in Section I-B.

B. Biomolecule Self-Assembly

Chemicals unless stated otherwise, were purchased from Sigma-Aldrich (St-Louis, MO). The silicon nanowires were functionalized by covalent attachment of anti-VEGF monoclonal antibody (R&D Systems, clone 26503) with GPTS (glycidoxypropyltrimethoxysilane) [24] using a modification of the procedure described by Kim *et al.* [25]. The silicon nanowire surface was cleaned with piranha 1:1 solution ($\text{H}_2\text{SO}_4/\text{H}_2\text{O}_2$), dried and incubated for 60 min at Room Temperature (RT) in

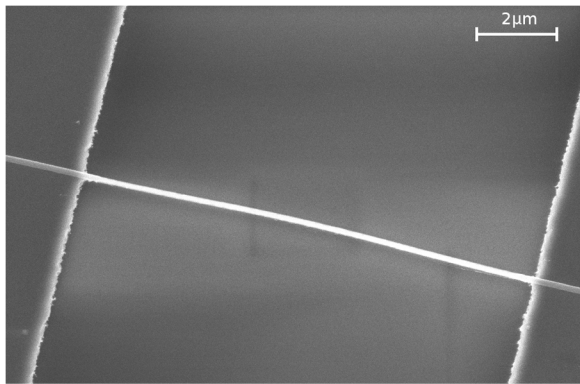


Fig. 2. Top SEM image of a single freestanding silicon NW.

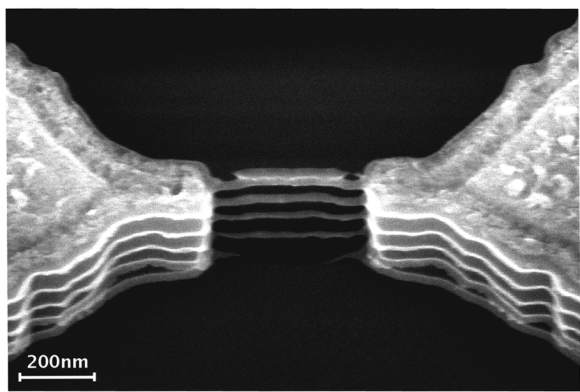


Fig. 3. Tilted SEM image of vertically stacked silicon nanowires.

ethanol containing 10 mM acetic acid and 1% GPTS. Following extensive washes with ethanol/acetic acid solution, the surface was dried under a N_2 stream and placed for 15 min at $110^\circ C$ in a dried oven. The surface was cooled down to RT and incubated overnight in a humid chamber at RT with Phosphate Buffer Saline (PBS) containing 0.5 mg/ml of anti-VEGF solution. The antibody solution was deposited onto the device both by standard drop casting with a Gilson pipette, and by a more precise one with the NanoInk's NLP 2000 System (Skokie, IL), an instrument capable of depositing materials with sub-micron accuracy and precision. Following extensive washes with PBS, the remaining active GPTS-derived groups were blocked by ethanolamine (10 mM ethanolamine, PH 8.0) for 60 min at RT. The excess of ethanolamine was removed by PBS washes and the surface blocked by an additional incubation with PBS containing 3% gelatin from cold water fish skin for 30 min at RT. The modified surface was washed and stored in PBS at $4^\circ C$ until use.

C. Surface SEM Imaging

Morphological analysis of the nano-structured electrodes was carried out using a Philips/FEI XL-30F microscope (The Netherlands), for acquiring Scanning Electron Microscopic (SEM) images for bare and bio-structured electrodes. Scanning electron microscope operating in ultra-high resolution (UHR) mode, with a working distance in the range 1.7–1.8 mm, was

used to analyze the morphology of SiNWs before and after the modification with anti-VEGF antibodies. The resolution used in UHR mode was 2.5 nm at 1 kV.

D. Fluorescence Tests

Characterization of the SiNW surface after bio-functionalization with a solution of fluorescein-labeled antibodies was performed by fluorescence. The optical fluorescence microscope used for imaging the proteins onto the device surface is an Eclipse LV 100 microscope. The objective is a Plan Fluor (50X magnification, $NA = 0.8$); the filter set is Cy5 designed for Alexa Fluor 647 compatible dyes (650 nm maximum excitation length, 668 nm maximum emission length). The camera used for imaging the fluorescence is a Nikon Digital Sight DS-2MBW.

E. I/V Measurements

To understand the effect of physical parameters on the silicon nanowires, several experiments were conducted by varying one parameter at a time during measurements. Although several parameters (temperature or geometry of the devices) can strongly influence the memristive bio-detection, in the present manuscript we more specifically focused on the humidity.

The memristive I/V characteristics were acquired by using the following equipment: Hewlett-Packard 4156A precision semiconductor parameter analyzer, Agilent Technologies Integrated Circuit Characterization and Analysis Program, Cascade Microtech Probe station, Nucleus Probe Station Control Software. The temperature was kept constant using feedback from the Rotronic HC2-C04 Thermo-Hygrometer tool, while varying the humidity. The Rotronic HW4 tool provided an accurate control of humidity and temperature of the measurement environment. A wet towel was introduced into the measurement chamber in order to raise the humidity, while its removal together with the utilization of silica gel was necessary to achieve a lower humidity. Every time, the measurements for each device were acquired before and after the surface modification with antibodies.

II. THEORY AND MODELS

A. Theory of the Memristive Effect

A memristor is a fundamental passive two-terminal circuit element whose conductivity varies with its state. Memristors intrinsically possess the capability of memory as they can maintain state. This effect is observed at the nano-scale where the current versus voltage characteristics appear as pinched hysteresis loops. The theory for a much broader range of systems showing this behavior was developed by Chua and Kang [26], [27]. These systems are known as memristive systems. They are passive systems that fall under the domain of non-linear circuit theory. To completely describe a memristive system, two equations are essential, as shown in (1), where \mathbf{w} represents a set of n state variables describing the device, and M , the memristance [26]:

$$\begin{aligned} \frac{d\mathbf{w}}{dt} &= f(\mathbf{w}, I, t), \\ V(t) &= M(\mathbf{w}, I, t)I(t). \end{aligned} \quad (1)$$

When the w depends only on charge, i.e. $w = q$, the memristor is said to be a pure memristor. Since the charge can vary in time, the state variable w can be expressed as:

$$\mathbf{w} = w(t) \quad (2)$$

The Hewlett-Packard (HP) memristor is the first physical implementation of the memristor [20]. The HP memristor is fabricated by using an annealed titanium dioxide (TiO_2) layer sandwiched between two platinum electrodes. Annealing is used to create oxygen vacancies. Oxygen vacancies are fundamental to the operation of the memristor, whose switching works on the principle of phase transition of TiO_2 . Strukov *et al.* [20] modeled the HP memristor as a device whose state is governed by the width of the depletion region. Assigning $w(t)$ as the actual width of the semiconductor layer and D as the thickness of the switching medium (TiO_2), they defined the voltage-to-current relation of charge controlled memristor by (3) [20]:

$$v(t) = \left(R_{ON} \frac{w(t)}{D} + R_{OFF} \left(1 - \frac{w(t)}{D} \right) \right) i(t) \quad (3)$$

were R_{ON} and R_{OFF} are the lowest and highest resistances that the memristor can attain respectively. The charge property of the device is obtained from (4) [20]:

$$\frac{dw(t)}{dt} = \mu_v \frac{R_{ON}}{D^2} i(t) \quad (4)$$

where μ_v represents the mobility of the oxygen vacancies. By inserting (4) into (3) the memristance $M(q)$ is defined as in (5) [20]:

$$M(q) = R_{OFF} \left(1 - \mu_v \frac{R_{ON}}{D^2} q(t) \right) \quad (5)$$

As the $M(q)$ results in a time depending value of the charge $q(t)$, the internal state variable of the device $w(t)$ is depending on the amount of charge that has moved through the memristor. $w(t)$ controls the overall resistance of the device and saturates with oxygen vacancies.

B. Standard Model

Williams' model [20] served as the main inspiration to the formulation of a theoretical model relevant to our silicon nanowire configuration. We named this model as standard model because it was derived directly from the Williams's theory and to distinguish it from the modified model described later. The standard model is based on the fundamentals of solid state physics and semiconductors. Central to its formation is the state variable $w(t)$, i.e. the total depletion width of (3) and (4). According to the technological features of the fabricated nanowires (Section I-A), the device is here considered as a 2-D block of silicon between two NiSi terminals, as depicted in Fig. 4. Region (1) represents crystalline silicon, while regions (2) represent nickel silicide. Regions (3) represent the depletion region. These two are formed due to the initial transfer of electrons from Si to NiSi. The uncovered charges create electric fields E_l and E_r , that oppose or support the external bias voltage, as shown in Fig. 4(a) and Fig. 4(b). To simplify the model a step further, the two depletion regions may be clumped

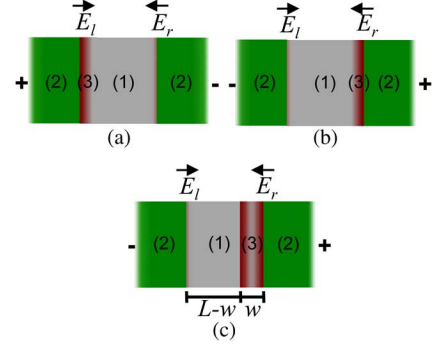


Fig. 4. Theory-w: device structure under forward (a) and backward (b) bias. (c) Simplified structure modeling of a memristive device.

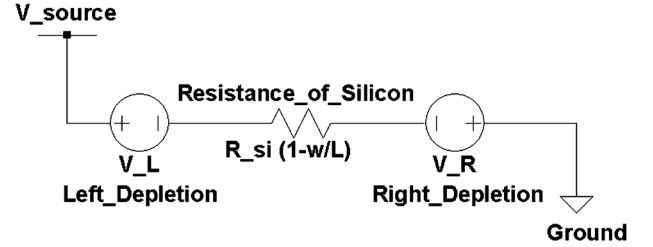


Fig. 5. Standard model: equivalent circuit.

into one region with width $w(t)$ but with opposite polarities as shown in Fig. 4(c). Here, we ignore the length of NiSi as it only contributes to series resistance and can be considered a current scaling component. The electronic circuit reported in Fig. 5 was used to model this structure and behavior.

The standard model can be described as a system of two equations. The first equation states that the rate of change of depletion width $w(t)$ is the drift velocity:

$$\frac{dw(t)}{dt} = a\mu_v E = \frac{a\mu_v V(t)}{L}, \quad (6)$$

where E is the net electric field, a is a proportionality or imperfection constant, μ_v is the mobility of free electrons in crystalline silicon, and $V(t)$ is the source voltage as a function of time. By solving the equation we can define the length $w(t)$ of the memristive element as:

$$w(t) = \frac{\mu_v(a\varphi(t) + b)}{L}, \quad (7)$$

with $\varphi(t)$ flux as a function of time and b the initial flux condition. For the second equation, we make the assumption that the difference in Schottky barrier heights of the left and right junctions is a linear function of the source voltage ((8)):

$$V_l - V_r = \gamma V(t) \quad (8)$$

By applying the Kirchhoff's Voltage law to the circuit of Fig. 5, the second equation of the system can be defined as:

$$V(t) - V_l + V_r - R_{Si} \left(1 - \frac{w(t)}{L} \right) i(t) = 0 \quad (9)$$

The solution of the system leads to the I/V equation:

$$i(t) = G(\varphi)V(t), \quad (10)$$

where $G(\varphi)$ is the memconductance.

By solving (10), and replacing the variable $w(t)$ of (7), the memconductance of the device can be derived:

$$G(\varphi) = \frac{(1 - \gamma)}{R_{Si} \left(1 - \frac{\mu_v(a\varphi(t)+b)}{L^2} \right)} \quad (11)$$

C. Phase Model

The memristive model described above did not show to fit properly our hysteretic curves, that were indeed manifesting an asymmetric behavior. From a pure phenomenological point of view, we decided to modify (6) by incorporating a phase component ϕ . This phase shift was added in order to better simulate the asymmetric behavior of our memristive silicon nanowires by stretching the hysteresis curve at one side. By replacing (7) by (12), and including the additional parameter, we defined the state variable of the model as:

$$w(t) = \frac{\mu(a\varphi(t + \phi) + b)}{L}, \quad (12)$$

where ϕ is the constant phase lead.

D. Equivalent Circuit Model

An equivalent circuit properly fitting the behavior of memristive silicon nanowires was also constructed (Fig. 6). The equivalent circuit model partly relies on reverse engineering studies on our memristive nanowires. Upon observations of current versus voltage curves, the forward and reverse characteristics of the fabricated devices closely resemble the I-V curves of a diode, but with different forward and backward cut-in voltages. The current versus time (I-t) characteristics provided a further insight into the nanowire current response, in the time-domain. I-t curves were extracted from the available data sets of measurements. Fig. 7 shows an example of voltage versus time (blue line) and current versus time (green line) characteristics from one silicon nanowire. The time responses of our memristive nanowires match well with the I-t characteristics of a diode too. All the devices showed to have similar I-t curves only varying in the amplitude and cut-in voltages. Thus, we can assume to implement the memristive effect of silicon nanowires by considering two different diodes: whenever one diode is forward biased the other one is reverse biased. The I-V characteristics of our nanowires can thus be modeled using a modified full wave rectifier circuit. A simple modification of the full-wave rectifier circuit enables us to introduce a phase difference between current and voltage via a capacitance (Fig. 6). The input to the diodes is modified by the capacitance and resistor combination. In the positive half cycle diode Df is active and it allows charge flow through it. However, during this half cycle diode, Dr is inactive and there is no current through Dr . In the negative half cycle the roles of the diodes are interchanged. Diode Dr is active whereas Df is reverse biased. Thus, there is current through Dr and no current through Df . The resistance R_{bias} simulates asymmetry observed in the characteristics. The shape of the curve may be fine tuned by varying the cut-in voltages of the diodes Df and Dr . Table I reports the equivalent circuit components and their effect on the memristive model.

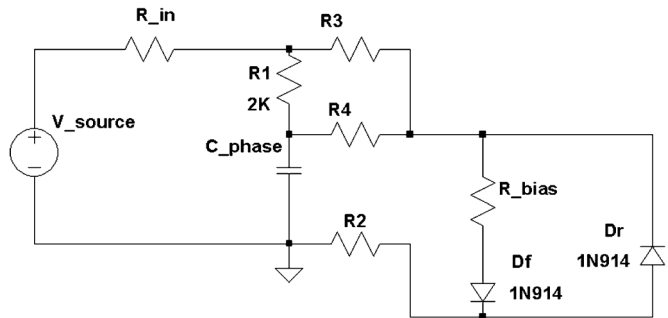


Fig. 6. Equivalent circuit.

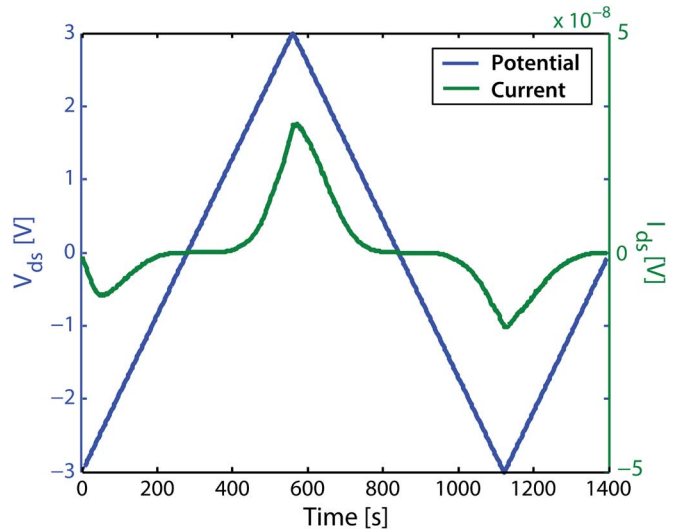


Fig. 7. Current and voltage versus time characteristics extracted from the data set of measurements related to silicon nanowire memristors.

TABLE I
EQUIVALENT CIRCUIT MODEL: COMPONENTS OF THE EQUIVALENT CIRCUIT AND THEIR EFFECT ON THE MEMRISTIVE MODEL

Component	Fitted component value
$R_{in}; R1; R2; R3; R4$	Series resistance, scaling the current
R_{bias}	Asymmetry
C_{phase}	Minima Gap
Df	Controls forward & decreasing characteristic
Dr	Controls reverse & increasing characteristic

III. RESULTS AND DISCUSSION

A. The Memristive Effects in Silicon Nanowires

Electrical measurements were carried out in order to characterize the memristive devices. They consist of the acquisition of the current flowing through the two terminals of the nanowire channel, as the source-drain current I_{ds} versus the potential V_{ds} applied to these terminals. As previously reported [21], the conductivity of the NW without any proteins immobilized on its top show a memristive effect. This is confirmed by the hysteretic values of the current for the same bias voltages (Fig. 8), and is probably related to the charge trapping mechanism at the Schottky junctions [28]. Fig. 9 reports an example of current minima acquired from an un-functionalized wire at room temperature and at $41.1 \pm 0.2\%$ of rH. The voltage gap measured between the forward (blue curve) and backward (red curve) current minima appears to be equal to zero for the bare nanowire

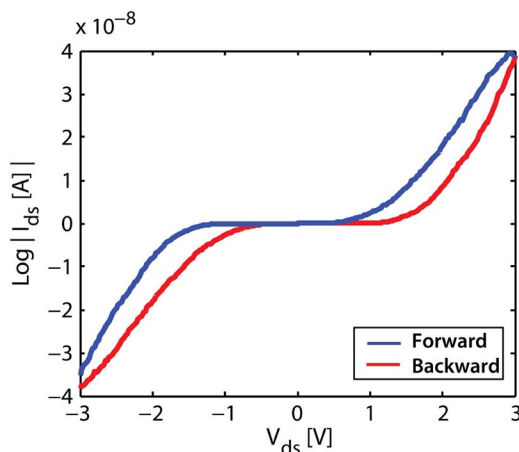


Fig. 8. Hysteretic I-V characteristic of a bare silicon nanowire. The blue curve represents the forward characteristic while the red one the backward one.

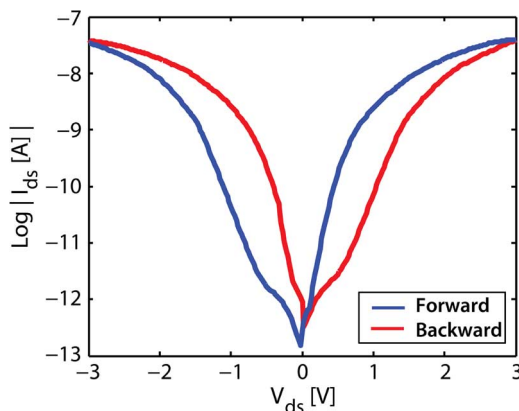


Fig. 9. Memristive silicon nanowire I-V characteristic in the logarithmic scale. Blue and red line stands for forward and backward current respectively. The minima voltage gap is characterized by small values in the case of bare nanowires.

in this relative humidity conditions. It has been also noticed that this value can vary quickly with the environmental conditions [19]. In particular the humidity changes can easily distort our experimental results. For this reason, an deep investigation of the humidity influence on nanowire measurements was carried out.

I/V measurements were acquired both on single freestanding nanowires and vertically stacked ones produced by either the original process and its variant. In both cases hysteresis characteristics were not showing relevant variations, but they were instead all similar to the one reported in Fig. 8. Also the behavior of the voltage gap parameter was comparable. That is the reason why we decided to test both kinds of wires, so that we could have a more important contribution to our statistical study.

B. Standard Model Simulations

The memristor model [20] was simulated in Matlab, and then compared to the acquired curves. Fig. 10 shows the match between the simulated and the experimental I/V characteristic, achievable by using the standard model explained in Section II-B. The continuous blue curve depicts the simulation results whereas the dashed black curve is the measured characteristic hysteresis acquired from a memristive nanowire. As we

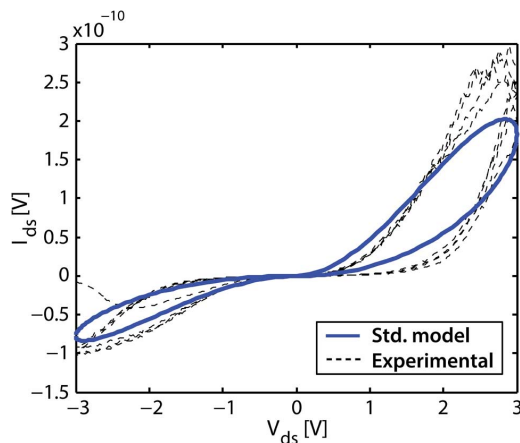


Fig. 10. Comparison of the standard model simulation with I/V measurement examples of a memristive device.

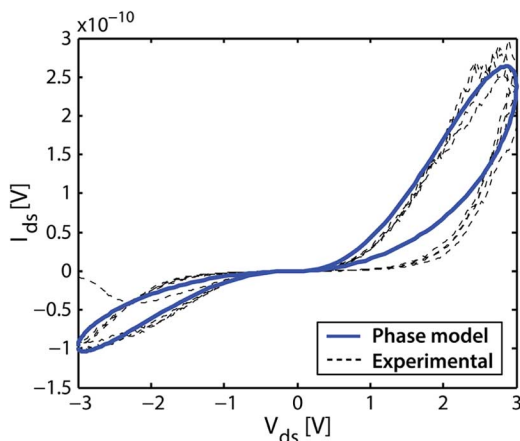


Fig. 11. Comparison of a simulation of the phase model with I/V measurements of memristive nanowire samples.

can see, the simulated curve reproduces the hysteretic shape of the experimental results. However, the standard model is not able to fully fit our data in terms of current maxima and threshold voltage.

C. Phase Model Simulations

The match was observed to improve after the addition of a fixed phase difference between the input voltage and the measured current (Section II-C). As is visible from Fig. 11, the modified phase model was found to closely resemble the measured I-V characteristics. The parameters of phase ϕ , forward cut-in b and reverse cut-in γ voltage were tuned to produce a close match. The mean absolute error measured was found to be 17.7 pA with a standard deviation of 0.3 pA. This evidences that our structures behave by following the memristor phenomenon up to an additive phase variable.

After humidity and temperature based experiments, it has been inferred that the ϕ , b and γ parameters have a dependence on temperature, humidity and dimensions of the device.

D. Equivalent Circuit Model Simulations

We report in Fig. 12 a comparison between an instance of the equivalent circuit with an experimental measurement from the device. The continuous curve represents the simulation results while the dashed curve represents the measured I curve. The

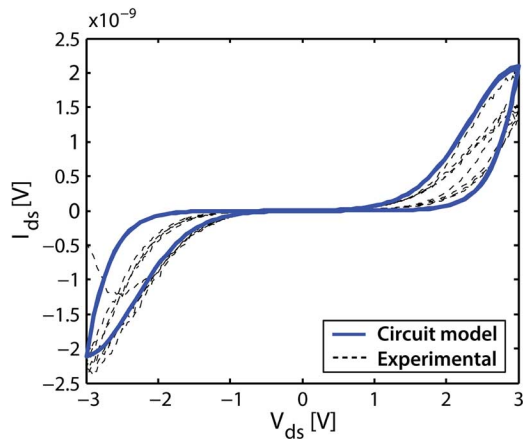


Fig. 12. Comparison of a simulation of the electrical inspired model with I/V measurements of memristive nanowires.

TABLE II
EQUIVALENT CIRCUIT MODEL: COMPONENTS OF THE EQUIVALENT CIRCUIT AND THEIR CORRESPONDING VALUES THAT BEST FIT THE EXPERIMENTAL $I_{ds} - V_{ds}$ CURVE OF FIG. 12

Component	Fitted component value
R_{in}	10 K Ω
$R1$	2 K Ω
$R2$	10 K Ω
$R3$	10 K Ω
$R1$	10 K Ω
R_{bias}	100 K Ω
C_{phase}	10 mF

model was developed by fitting the parameters of the equivalent circuit of Fig. 6 with the experimental curves.

Table II reports the values chosen for each component of the equivalent circuit (Table I) that have led to the fitted curve of Fig. 12. The comparison between the simulated circuit curves and the experimental ones shown in Fig. 12 was made with measurements acquired from seven devices characterized by same dimensions. The comparison has revealed a mean absolute error of 20.7 nA, and a standard deviation of 1.1 nA. As we can see, the equivalent circuit fits better the memristive effect of our silicon nanowires. Even in this case, the additional introduction of a phase parameter C_{phase} was needed to enhance the similarity; it enabled a better comparison with the hysteretic shape.

The diode based circuit is only an equivalent circuit model of the memristive silicon nanowires. It hides all the nano-scale effects and only attempts to emulate the device behavior. Nevertheless, this equivalent circuit relies on theory of p-n junction diodes which already have well developed theories and, thus, can be easily implemented in any circuit simulator. For this particular simulation LTspice IV simulator was used.

E. SEM Imaging on Nanowire Biosensor

Fig. 13 and Fig. 14 depict the acquired SEM images for one bare silicon nanowire and for a nanowire surface modified with a biomolecular layer, respectively. The memristor channel was modified with a layer of anti-VEGF antibody (Fig. 14). The nanowire before and after the bio-functionalization shows a significant difference in diameter. Repeating observations of SEM images taken from different NWs lead to the calculation of a mean diameter of 118.7 ± 12.5 nm and of 145.8 ± 3.7 nm for

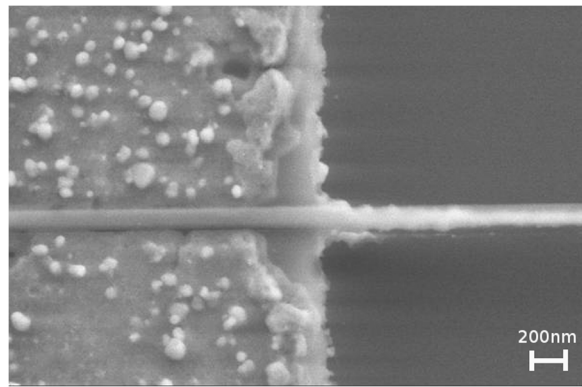


Fig. 13. SEM image of the surface of a bare memristive nanowire.

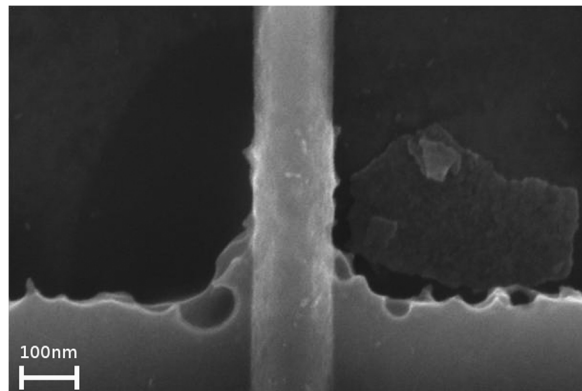


Fig. 14. SEM image of the surface of a memristive nanowire modified with biomolecules.

bare nanowires and bio-modified nanowires, respectively. Thus, these data confirm the successful monolayer self-assembly at the silicon surface of the nanowire.

F. Fluorescence Imaging

Further characterization tests based on fluorescence imaging were used to test the presence of antibody proteins drop casted onto the SiNW surface (Section II-D). Fig. 15 represents the bright field, zoomed-in microscope image of one of the fabricated devices functionalized by using the nano-spotting. The reported fluorescence image is a zoomed view of the nanowire, and clearly shows the fluorescence emitted by the antibody-coating layer deposited onto the SiNW. This result further confirms the presence of the proteins onto the sensor, and is in agreement with the varying electrical properties of the SiNWs that will be described in next sections.

G. Enhanced Voltage Minima Gap After Bio-Functionalization

Fig. 16 shows the logarithmic source-drain current versus the bias potential in the case of functionalized nanowire, acquired at room temperature and at $41.1 \pm 0.2\%$ of humidity. The surface modification with anti-VEGF antibody was done with the procedure reported in Section I-B. Unlike bare wires, showing small voltage gap values (Fig. 9), functionalized memristors tested under similar humidity show different positions of the current minima for backward and forward regimes (Fig. 16), consistently with previously reported measurements [29]. The increased minima voltage gap can be identified with the memory

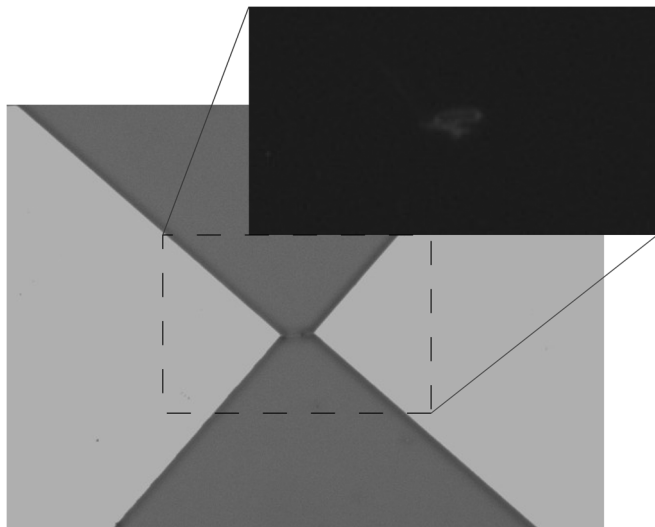


Fig. 15. Fluorescence microscope image in zoom view of the antibody layer deposited onto the SiNW surface.

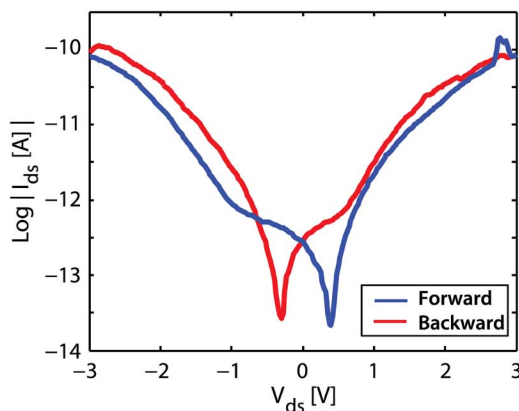


Fig. 16. $\text{Log}|I_{ds}| - V_{ds}$ curves showing the increased minima voltage gap after the bio-functionalization.

storage of the memristive nanowires as driven by charges made by antibody functionalization [19].

The covalent attachment of antibodies all-around to the source-drain channel produces a conductance change in the corresponding silicon nanowire device. From an electrical point of view, the protein coverage can be seen as a virtual all-around gate that controls the channel current. As already well known, in the case of a p-type (boron-doped) silicon nanowire, as the one that we fabricate, applying a positive gate voltage depletes carriers and reduces the conductance, whereas applying a negative gate voltage leads to an accumulation of carriers and an increase in conductance. In our case, the conductance depends on the charged species bound to the channel surface when a potential is applied to the nanowire. Since each protein carries on charged residues, the conductance of a p-silicon nanowire will increase (decrease) when a protein with negative (positive) surface charge binds to the channel. Antibodies show a net contribution of positively charged residues that acts by creating an electric field surrounding the source-drain channel of our memristive biosensor [19]. As a consequence, unlike un-functionalized Si nanowires showing memristive $I_{ds} - V_{ds}$

characteristic with zero-crossing at small V_{ds} , the voltage gap after bio-functionalization appears increased (Fig. 16).

H. The Role of Humidity in the Memristive Bio-Detection

As already mentioned in Section III-A, the current properties of the measured samples can be strongly affected by humidity. Silicon nanowires show in itself a relevant dependence on humidity [30], [31]. In fact, due to the large surface-to-volume ratio, they present a large amount of hydroxyl groups that enable the adsorption of more water molecules. This makes the surface highly hydrophilic, determining the high sensitivity to humidity. Also dried organic samples have shown to be affected by water molecules adsorbed from humid environment [23].

In order to study the effect of water molecules on the hysteretic current, nanowire biosensors were tested under different conditions of humidity. Functionalized devices were kept in buffered solution before their utilization for I/V measurements. Then the devices were gently dried under a nitrogen flow, and loaded inside a sealed measurement chamber, where they were left for about 20 minutes in order to get steady equilibrium condition. Before measuring, a sensor recording the chamber humidity was positioned inside the chamber. A wet towel introduced inside the measurement chamber allowed us to raise the humidity; whereas, the use of silica gel and temperature ramp applied to the wafer holder were used to drop it down. When the humidity was stable, $I_{ds} - V_{ds}$ curves were acquired from one device at one time. In order to investigate the effect of the air relative humidity, repeated acquisitions were performed on same nanowires but at increasing rH. For this aim, vertically stacked silicon nanowires characterized by same fabrication process and chemical treatment were tested. Different effects were found in bare wires and bio-modified ones. The change in relative humidity affects the source-drain current I_{ds} in a way still unpredictable. Due to the large statistical error affecting current measurements, a clear analysis of the modifications in the hysteretic current peaks as function of the humidity could not be achieved. Instead, the changes in the minima voltage gap parameter followed a well reproducible behavior in devices characterized by the same functionalization and the same dimensions.

In Fig. 17, the effect of humidity on the minima voltage gap are presented in the two cases of nanowires measured before and after functionalization with anti-VEGF antibodies. In order to have a statistical measurement of this behavior, the voltage gap was measured on 20 identical wires, before and after the bio-functionalization, in three different humidity conditions. Bare NWs were tested at $41.1 \pm 0.2\%rH$, $45.7 \pm 0.3\%rH$ and $57.9 \pm 0.4\%rH$; the same ones but with bio-modified surface at $30.2 \pm 0.1\%rH$, $45.5 \pm 0.1\%rH$ and $59.5 \pm 0.2\%rH$. The control of the humidity during the acquisition was not trivial. We did it by inserting a wet towel in the measurement chamber as described in Section I-E. Because of that, the $I_{ds} - V_{ds}$ curve acquisition from same memristive devices, before and after the functionalization, could not be performed exactly at the same rH values, but similar humidity windows were taken into account. The reported voltage gap values were calculated from $I_{ds} - V_{ds}$ characteristics related to nanowire devices with a length of 120 nm and a diameter of 30 nm. Data were acquired at an average

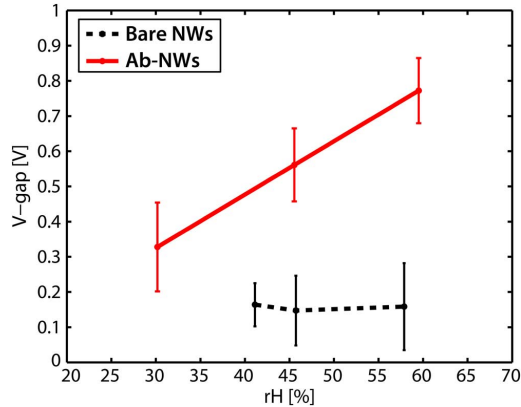


Fig. 17. Calculated average voltage minima gap as function of the humidity in vertically stacked nanowires.

temperature of 23°C. Each voltage gap point was calculated as the mean value obtained by testing once each of the 20 devices under same humidity.

The first important observation evident from this graph is the different behavior expressed by nanowires with and without surface modification. If we compare data related to the memristive effect before (black dashed line) and after anti-VEGF functionalization of the same wires (red solid line), we can easily see that the minima voltage gap is roughly constant in the case of bare devices, and very close to zero. The reported error bars describe the deviation of the voltage gap measured in 20 NWs from the ideal case that is 0 Volts in bare memristive devices. The constant, quasi-zero behavior is a relevant finding, because it shows the stability of our biosensor prior to any modification in the surrounding humid environment.

Secondly, a certain degree of inter-device variability is present. The error bars of Fig. 17 define the standard deviation calculated on the 20 devices, before and after the surface modification, respectively; each of them was tested once under a fixed humidity. This variability can be attributed to defects easily insertable with fabrication processes not fully repeatable, or to non homogeneous distribution of biological species in functionalized nanowires. Moreover, a slight change induced by humidity variations is consistent, as it is well known that raw silicon surfaces are normally covered by many Si-OH chemical bonds. Because these pending groups enable weak interactions with H₂O molecules present in the surrounding air environment, they can lead to a changing response time and hysteresis curve [31].

Nevertheless, most of the wires behaved the same way when tested at fixed humidity conditions, as confirmed by superimposed $I_{ds} - V_{ds}$ characteristics. Fig. 18 shows an example of 20 different devices tested under an humidity of $59.5 \pm 0.2\%$ and a temperature of $24.1 \pm 0.1^\circ\text{C}$. The reported data can be thus considered as an important evidence of the good reproducibility of our memristive biosensor.

Finally, each device of Fig. 18 shows a clear voltage gap between the forward and backward current minima of the hysteresis, demonstrating the presence of a biomolecular layer on the wire surface. As represented by the graph in Fig. 17, the voltage gap fluctuations when varying the humidity conditions clearly appear strongly amplified when antibody-modified

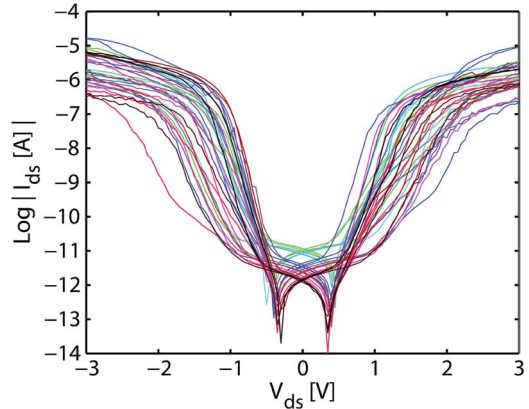


Fig. 18. Voltage gap reproducibility. Minima voltage gap as function of the humidity calculated for 20 memristive vertically stacked silicon nanowires. The nanowires were functionalized with anti-VEGF antibodies.

nanowires are measured, enabling the identification of bio-molecule interactions at the surface of our nanowires. This fact confirms data from Fig. 16 where the distance between the forward and backward minima current of two nanowires is enhanced when tested after the functionalization process. Fig. 17 also validates the previous findings about the increased responses of memristive nanowires with antibody uptake [19]. At a biochemical level, the observed behaviors can already find a first explanation. Anti-human VEGF antibody is a protein containing -S, =O and -N terminal groups that can create bonds with water molecules. N—O and S—H interactions are known to be much stronger than the ones existing between Si and -OH groups, and can be one of the main reasons explaining how the detection parameter, the voltage gap, can differ between the two cases. Furthermore, looking at the minima voltage gap acquired from the $I_{ds} - V_{ds}$ characteristics of functionalized NWs, the changing voltage gap is clearly following a steep increasing behavior. In particular, the red line in Fig. 17 demonstrates that the gap in potential between the hysteresis minima of memristive anti-VEGF modified nanowires linearly increases as function of the humidity within the investigated range from $30.2 \pm 0.1\%$ to $59.5 \pm 0.2\%$ rH. This phenomenon is perfectly according with the finding that organic film can adsorb water molecules from the surrounding humid environment [23], resulting in an increased modification of the charge distribution at the silicon nanowire surface when a potential is applied. A relevant statistical contribution to this study was also made by $I_{ds} - V_{ds}$ measurements performed on single free-standing NWs. They also showed a comparable voltage gap behavior if the same range of humidity investigated here was considered.

IV. CONCLUSION

In this paper we presented nanowires fabricated on Silicon-on-Insulator wafers. Free-standing nanowires have been obtained by using a chemical etching process on preformed wires by E-beam Lithography. Anti-human VEGF proteins have been used to functionalized the free-standing wires. The electrical properties of the nanowires have been acquired on humid air, and have been found to manifest memristive conductivity. The memristive effect has been confirmed by both a state-variable model and an equivalent circuit model.

The equivalent circuit is also designed in order to simulate the component behavior with the tool LTSpice IV. The memristive effect is also registered by a voltage gap measured on the current-to-voltage characteristics. However, our findings demonstrate that this voltage gap is largely affected by the relative humidity of the measuring chamber. A series of measurements performed on nanowires from the same fabrication process and under the same relative humidity allowed us to record statistically robust trends in voltage variations. Different behaviors have been acquired on bare and functionalized wires. Data confirm the stability of silicon free-standing nanowires under changing environment conditions. Specifically, the current/voltage measurements demonstrate that the memristive effect is affected by the relative humidity surrounding functionalized nanowires; the antibody layer onto the nanowire sensor surface is confirmed by the increased voltage gap of bio-modified wires with respect to the measurements in bare NWs. At high humidity values this difference between voltage gap in the bare and functionalized case is enhanced, due to the higher affinity of proteins for water molecules. The proposed memristive sensor is calibrated in humidity and can thus be used for biosensing.

ACKNOWLEDGMENT

The work was in part supported by the multidisciplinary FNS grant (CR3213 135073) and by an ERC grant (ERC-2009-Adg-246810). This work was also partially supported by the Nano-Tera grants no. 20NA21-128841 and no. 20NA21-128840, evaluated by the Swiss NSF foundation. The authors would like to thank Robert Stokes from NanoInk (Skokie, IL, USA) for the nano-spotting of antibodies onto the devices.

REFERENCES

- [1] U. Yogeswaran, S. Thiagarajan, and S. Chen, "Nanocomposite of functionalized multiwall carbon nanotubes with nafion, nano platinum, nano gold biosensing film for simultaneous determination of ascorbic acid, epinephrine, uric acid," *Anal. Biochem.*, vol. 365, pp. 122–131, 1999.
- [2] J. Hubalek, J. Hradecky, V. Adam, O. Krystofova, M. Masarik, L. Trnkova, A. Horna, K. Klosova, M. Adamek, K. Zehnalek, and R. Kizek, "Spectrometric and voltammetric analysis of urease nickel nanoelectrode as an electrochemical sensor," *Sensors*, vol. 7, pp. 1238–1255, 2007.
- [3] U. Yogeswaran, S. Thiagarajan, and S. Chen, "Pinecone shape hydroxypropyl- β -cyclodextrin on a film of multi-walled carbon nanotubes coated with gold particles for the simultaneous determination of tyrosine, guanine, adenine and thymine," *Carbon*, vol. 45, pp. 2783–2796, 2007.
- [4] U. Yogeswaran and S. Chen, "Electrocatalytic properties of electrodes which are functionalized with composite films of f-MWCNTs incorporated with poly(neutral red)," *J. Electrochem. Soc.*, vol. 154, pp. E178–E186, 2007.
- [5] C. Boero, S. Carrara, G. Del Vecchio, L. Calza, and G. De Micheli, "Highly sensitive carbon nanotube-based sensing for lactate and glucose monitoring in cell culture," *IEEE Trans. NanoBiosci.*, vol. 10, p. 1, 2011.
- [6] T. Kuila, S. Bose, P. Khanra, A. Mishra, N. Kim, and J. Lee, "Recent advances in graphene-based biosensors," *Biosens. Bioelectron.*, vol. 26, no. 12, pp. 4637–4648, 2011.

- [7] C. Li, M. Curreli, H. Lin, B. Lei, F. Ishikawa, R. Datar, R. Cote, M. Thompson, and C. Zhou, "Complementary detection of prostate-specific antigen using In_2O_3 nanowires and carbon nanotubes," *J. Amer. Chem. Soc.*, vol. 127, pp. 12 484–12 485, 2005.
- [8] Z. Zhao, X. Zhang, B. Wang, and H. Jiang, "ZnO-based amperometric enzyme biosensors," *Sensors*, vol. 10, pp. 1216–1231, 2010.
- [9] G. Zheng, F. Patolsky, Y. Cui, W. Wang, and C. Lieber, "Multiplexed electrical detection of cancer markers with nanowire sensor arrays," *Nat. Biotechnol.*, vol. 23, no. 3, pp. 1294–1301, 2005.
- [10] F. Patolsky, G. Zheng, and C. Lieber, "Nanowire sensors for medicine and the life sciences," *Nat. Biotechnol.*, vol. 1, no. 1, pp. 51–65, 2006.
- [11] D. A. Giljohann and C. Mirkin, "Drivers of biodiagnostic development," *Nature*, vol. 462, pp. 461–464, 2009.
- [12] F. Patolsky and C. Lieber, "Nanowire nanosensors," *Mater. Today*, vol. 8, no. 4, pp. 20–28, 2005.
- [13] F. Patolsky, G. Zheng, and C. Lieber, "Fabrication of silicon nanowire devices for ultrasensitive, label-free, real-time detection of biological and chemical species," *Nat. Protoc.*, vol. 1, pp. 1711–1724, 2006.
- [14] X. Zhou, J. Hu, C. Li, D. Ma, and S. Lee, "Silicon nanowires as chemical sensors," *Chem. Phys. Lett.*, vol. 369, pp. 220–224, 2003.
- [15] A. Wanekaya, W. Chen, N. Myung, and A. Mulchandani, "Nanowire-based electrochemical biosensors," *Electroanal.*, vol. 18, no. 6, pp. 533–550, 2006.
- [16] J. Janata and M. Josowicz, "Conducting polymers in electronic chemical sensors," *Nat. Mater.*, vol. 2, pp. 19–24, 2003.
- [17] Y. Cui, Q. Wei, H. Park, and C. Lieber, "Nanowire nanosensors for highly sensitive and selective detection of biological and chemical species," *Science*, vol. 293, pp. 1289–1292, 2001.
- [18] E. Stern, A. Vacic, and A. Mark, "Semiconducting nanowire field-effect transistor biomolecular sensors," *IEEE Trans. Electron Devices*, vol. 55, no. 11, pp. 3119–3130, 2008.
- [19] S. Carrara, D. Sacchetto, M.-A. Doucey, G. De Micheli, and Y. Leblebici, "Memristive-biosensors: A new detection method by using nanofabricated memristors," *Sens. Actuators B*, vol. 171–172, pp. 449–457, 2012.
- [20] D. Strukov, G. Snider, D. Stewart, and R. Williams, "The missing memristor found," *Nature*, vol. 453, no. 7191, pp. 80–83, 2008.
- [21] D. Sacchetto, M.-A. Doucey, G. De Micheli, Y. Leblebici, and S. Carrara, "Multiplexed electrical detection of cancer markers with nanowire sensor arrays," *BioNanoSci.*, vol. 1, pp. 1–3, 2011.
- [22] F. Corinto and A. Ascoli, "A boundary condition-based approach to the modeling of memristor nanostructures," *IEEE Trans. Circuits Syst. I, Reg. Papers*, vol. 59, no. 11, pp. 2713–2726, 2012.
- [23] S. Carrara, V. Erokhin, and C. Nicolini, "Stm image formation of organic thin films: The role of water shell," *Physica E*, vol. 16, no. 16, pp. 6577–6582, 2000.
- [24] A. Kusnezow, A. Walijew, F. Diehl, and J. Hoheisel, "Antibody microarrays: An evaluation of production parameters," *Proteomics*, vol. 3, no. 3, pp. 254–264, 2003.
- [25] D. Kim, H. Lee, H. Jung, and S. Kang, "Single-protein molecular interactions on polymer-modified glass substrates for nanoarray chip application using dual-color tirm," *Bull. Korean Chem. Soc.*, vol. 28, no. 5, pp. 783–790, 2007.
- [26] L. Chua and S. Kang, "Memristive devices and systems," *Proc. IEEE*, vol. 64, no. 2, pp. 209–223, 1976.
- [27] L. Chua, "Memristor—the missing circuit element," *IEEE Trans. Circuit Theory*, vol. CT-18, pp. 507–519, 1971.
- [28] N. Archontas, J. Georgiou, M. H. B. Jamma, S. Carrara, and G. D. Micheli, "Characterization of memristive poly-si nanowires via empirical physical modelling," in *Proc. ISCAS'10*, pp. 1675–1678.
- [29] D. Sacchetto, M. Ben-Jamaa, S. Carrara, G. De Micheli, and Y. Leblebici, "Memristive devices fabricated with silicon nanowire schottky barrier transistors," in *Proc. ISCAS*, 2010, pp. 9–12.
- [30] H. Li, J. Zhang, B. Tao, L. Wan, and W. Gong, "Investigation of capacitive humidity sensing behavior of silicon nanowires," *Langmuir*, vol. 41, pp. 600–604, 2009.
- [31] X. Chen, J. Zhang, Z. Wang, and S. Hui, "Humidity sensing behavior of silicon nanowires with hexamethyldisilazane modification," *Sens. Actuators B*, vol. 156, pp. 631–636, 2011.



Francesca Puppo received the B.S. degree in biomedical engineering and the M.S. degree (cum laude) in bioengineering, both from the University of Genoa, Italy, in 2008 and 2011 respectively. She carried out her Master thesis at the Integrated System Laboratory (LSI) of EPFL (Switzerland) in collaboration with the Department of Electrical Engineering and Biophysics (DIBE) of the University of Genoa, Italy. She worked on the design and the fabrication of a CNTFET-based biosensor. She also interned at LSI for a five-month project based

on the study of Silicon Nanowire based biosensors. Currently she is working as a Ph.D. student in Microsystems and Microelectronics in the Integrated System Laboratory (LSI) of EPFL, under the supervision of Sandro Carrara and Giovanni De Micheli. Her research focuses on the design and fabrication of novel memristive-biosensor based on silicon nanowires (SiNWs).



Akshat Dave received his B.S. degree from Nanyang Technological University (NTU), Singapore, in 2012 with a research exchange at EPFL in 2011. While at NTU, he has worked on a wide range of topics ranging from computer vision, machine learning and pattern recognition to nanobiosensing. His current research interests include mathematical modeling and algorithm design for applications in healthcare and social science.



Marie-Agnès Doucey received a Ph.D. in biochemistry from Friedrich-Miescher Institute at Novartis, Basel, Switzerland. She also holds a degree in Engineer in Biotechnology received at the Ecole Supérieure de Biotechnologies de Strasbourg (ESBS), France. She is currently a project leader at the Ludwig Institute for Cancer Research at the University of Lausanne. Her current work focuses on the tumor microenvironment and the role of monocytes in breast cancer tumor development. She has more than twenty publications in peer-reviewed

international journals.



Davide Sacchetto received the B.S. degree in physics engineering from Politecnico di Torino, Italy, in 2007. In 2008 he received the jointed M.S. degree in micro and nano technologies for integrated systems from Ecole Polytechnique Fédérale de Lausanne (EPFL), the Institut National Polytechnique de Grenoble (INPG), and the Politecnico di Torino (POLITO). He received his Ph.D. degree in microsystems and microelectronics in September 2013 from EPFL. His research interests focus on novel devices, investigating issues ranging from

solid-state microfabrication to circuit implementation. He is interested in the post-processing fabrication of CMOS technology that can enable integration of CMOS with the additional functionality that emerging technology can bring. For instance, resistive RAM devices integrated with CMOS can bring performance benefits to diverse CMOS applications, such as FPGAs, artificial neural networks, standalone memories.



Camilla Baj-Rossi received a B.S. degree in 2008 and a M.S. degree in 2010 in biomedical engineering at Politecnico di Torino, Italy. She carried out her master's project at EPFL in the Integrated System Laboratory (LSI), working on the design of a multi-panel biochip based on P450 and CNT for drugs monitoring in personalized therapy. Currently she is a Ph.D. student in microsystems and microelectronics in the Integrated System Laboratory (LSI) under the direction of Sandro Carrara and Giovanni De Micheli.



Yusuf Leblebici (F'10) received his B.Sc. and M.Sc. degrees in electrical engineering from Istanbul Technical University, Turkey, in 1984 and 1986, respectively, and his Ph.D. degree in electrical and computer engineering from the University of Illinois at Urbana-Champaign, IL, USA (UIUC) in 1990. Between 1991 and 2001, he worked as a faculty member at UIUC, at Istanbul Technical University, and at Worcester Polytechnic Institute (WPI). In 2000–2001, he also served as the Microelectronics Program Coordinator at Sabanci University. Since

2002, Dr. Leblebici has been a Chair Professor at the Swiss Federal Institute of Technology in Lausanne (EPFL), and director of Microelectronic Systems Laboratory. His research interests include design of high-speed CMOS digital and mixed-signal integrated circuits, computer-aided design of VLSI systems, intelligent sensor interfaces, modeling and simulation of semiconductor devices, and VLSI reliability analysis. He is the coauthor of four textbooks, namely, *Hot-Carrier Reliability of MOS VLSI Circuits* (Kluwer Academic Publishers, 1993), *CMOS Digital Integrated Circuits: Analysis and Design* (McGraw Hill, 1st Ed. 1996, 2nd Edition 1998, 3rd Edition 2002), *CMOS Multichannel Single-Chip Receivers for Multi-Gigabit Optical Data Communications* (Springer, 2007), and *Fundamentals of High Frequency CMOS Analog Integrated Circuits* (Cambridge University Press, 2009), as well as more than 200 articles published in various journals and conferences. He has served as an Associate Editor of IEEE TRANSACTIONS ON CIRCUITS AND SYSTEMS—PART II, and IEEE TRANSACTIONS ON VERY LARGE SCALE INTEGRATED (VLSI) SYSTEMS. He has also served as the general co-chair of the 2006 European Solid-State Circuits Conference, and the 2006 European Solid State Device Research Conference (ESSCIRC/ESSDERC). He was elected as Distinguished Lecturer of the IEEE Circuits and Systems Society for 2010–2011.



Giovanni De Micheli (F'94) received a Nuclear Engineer degree from Politecnico di Milano, Italy, in 1979 and the M.S. and Ph.D. degrees in electrical engineering and computer science from the University of California at Berkeley, CA, USA, in 1980 and 1983, respectively. He is Professor and Director of the Institute of Electrical Engineering and of the Integrated Systems Centre at EPF Lausanne, Switzerland. He is program leader of the Nano-Tera.ch program. Previously, he was Professor of Electrical Engineering at Stanford University.

Prof. De Micheli is a Fellow of ACM and a member of the Accademia Europaea. His research interests include several aspects of design technologies for integrated circuits and systems, such as synthesis for emerging technologies, networks on chips and 3-D integration. He is also interested in heterogeneous platform design including electrical components and biosensors, as well as in data processing of biomedical information. He is author of: *Synthesis and Optimization of Digital Circuits* (McGraw-Hill, 1994), co-author and/or co-editor of eight other books and of over 500 technical articles. His citation h-index is 81 according to Google Scholar. He is member of the Scientific Advisory Board of IMEC and STMicroelectronics. Prof. De Micheli is the recipient of the 2012 IEEE/CAS Mac Van Valkenburg award for contributions to theory, practice and experimentation in design methods and tools and of the 2003 IEEE Emanuel Piore Award for contributions to computer-aided synthesis of digital systems. He received also the Golden Jubilee Medal for outstanding contributions to the IEEE CAS Society in 2000, the D. Pederson Award for the best paper on the IEEE Transactions on CAD/ICAS in 1987, and several Best Paper Awards, including DAC (1983 and 1993), DATE (2005), and Nanoarch (2010 and 2012). He has been serving IEEE in several capacities, namely: Division 1 Director (2008–9), co-founder and President Elect of the IEEE Council on EDA (2005–7), President of the IEEE CAS Society (2003), Editor-in-Chief of the IEEE TRANSACTIONS ON COMPUTER-AIDED DESIGN OF INTEGRATED CIRCUITS AND SYSTEMS (1997–2001). He has been Chair of several conferences, including DATE (2010), pHealth (2006), VLSI SOC (2006), DAC (2000), and ICCD (1989).



Sandro Carrara (M'09) is Lecturer at EPFL, Lausanne, Switzerland. He is former Professor of optical and electrical biosensors at the Department of Electrical Engineering and Biophysics (DIBE) of the University of Genoa, Italy, and former Professor of nanobiotechnology at the University of Bologna, Italy. He is founder and Editor-in-Chief of the journal *BioNanoScience* by Springer, Topical Editor of the IEEE SENSORS JOURNAL, and Associate Editor of IEEE TRANSACTIONS ON BIOMEDICAL CIRCUITS AND SYSTEMS. He is an IEEE member for the Circuit and System Society (CASS) and member of the Board of Governors of the IEEE Sensors Council. He has been appointed as CASS Distinguished Lecturer for the years 2013–2014. His scientific interests are on electrical phenomena of nano-bio-structured films, and include CMOS design of biochips based on proteins and DNA. He has more than 160 scientific publications and 12 patents. He has several Top-25 Hottest-Articles (2004, 2005, 2008, 2009, and two times in

2012) published in highly ranked international journals such as *Biosensors and Bioelectronics*, *Sensors and Actuators B*, IEEE SENSORS JOURNAL, and *Thin Solid Films*. His work received a NATO Advanced Research Award in 1996 for the original contribution to the physics of single-electron conductivity in nano-particles, two Best Paper Awards at the IEEE PRIME Conference in 2010 (Berlin), and in 2009 (Cork), a Best Poster Award at the Nanotera workshop in 2011 (Bern), and a Best Poster Award at the NanoEurope Symposium in 2009 (Rapperswil). He also received the Best Referees Award from the journal *Biosensor and Bioelectronics* in 2006. From 1997 to 2000, he was a member of an international committee at the ELETTRA Synchrotron in Trieste. From 2000 to 2003, he was scientific leader of a National Research Program (PNR) in the field of nanobiotechnology. He is now an internationally esteemed expert of the evaluation panel of the Academy of Finland in a research program for the years 2010–2013. He is the General Chairman of the Conference IEEE BioCAS 2014.